Supplementary Materials for

Gut microbiota dysbiosis orchestrates vitiligo-related oxidative stress through the metabolite hippuric acid

Qingrong Ni *et al.*

Corresponding author: Jing Huang, jinghuang@fmmu.edu.cn; Hong Cai, ch1031@163.com; Qingrong Ni, niqingrong@fmmu.edu.cn

The PDF file includes:

Other Supplementary Material for this manuscript includes the following:

Fig. S1. Lesional skin signature in vitiligo patients. Heatmap of the top 190 differentially expressed genes (DEGs) in lesional versus non-lesional skin. Each column represents a biological replicate, and each row represents a gene.

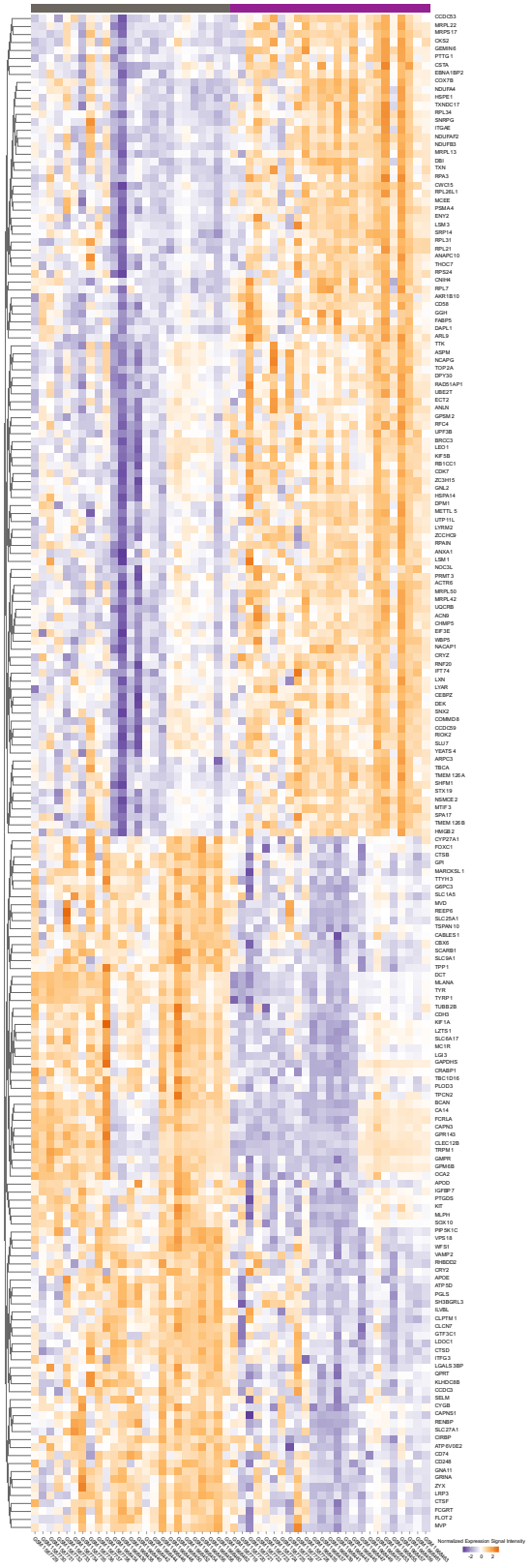

Fig. S2. Tail Skin transcriptome signature in the melanoma-Treg-induced vitiligo mouse model. (**A**) Representative images of tail skin hair from mice at Day 0, Day 35, and Day 60 post melanoma/Treg-induced vitiligo induction procedure. (**B**) Heatmap of the top 150 differentially expressed genes (DEGs) in the tail skin of non-induction (n = 9) and vitiligo (n = 9) mice. Each column represents a biological replicate.

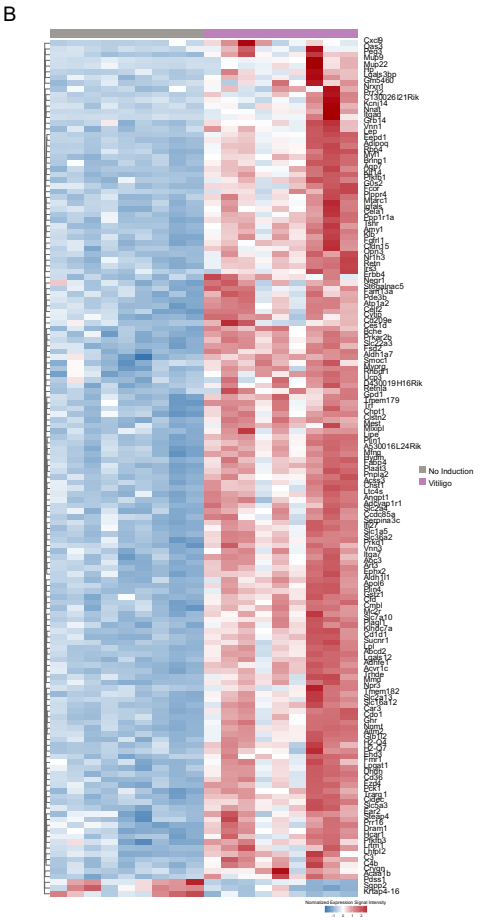

Fig. S3. Tail skin signature between vitiligo mice treated with water and ABX. Heatmap of the top 150 differentially expressed genes (DEGs) in the tail skin of non-induction (n = 6) and vitiligo (n = 6) mice. Each column represents a biological replicate.

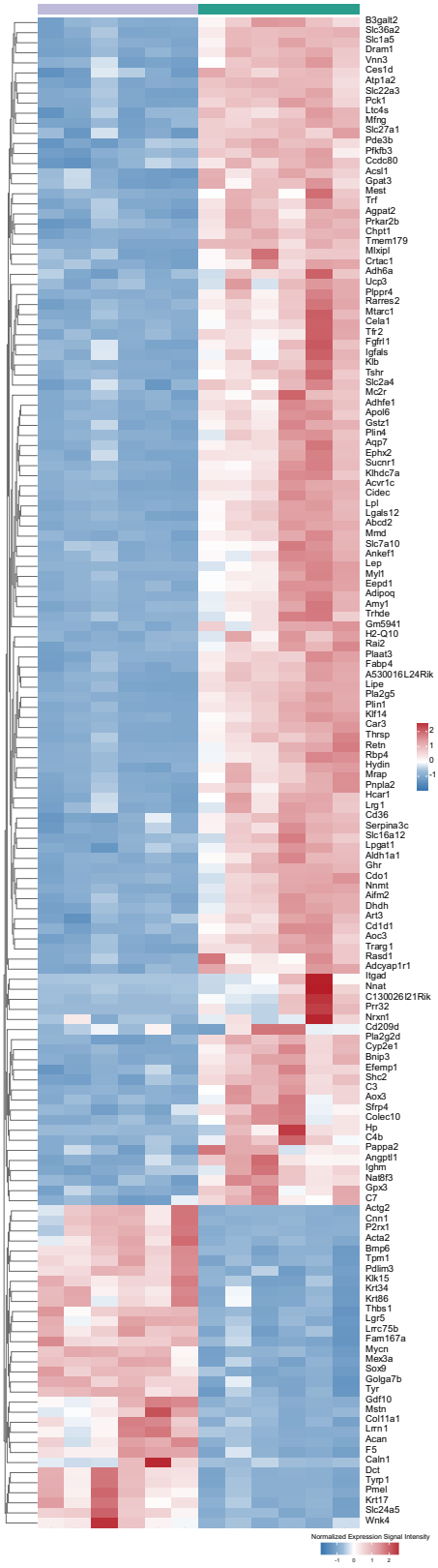

Fig. S4. Gut dysbiosis signature of vitiligo mice after melanoma-Treg-induced vitiligo model. (**A**) Bar chart showing the relative abundance of microbiota at the *family* level in fecal samples from non-induction ($n = 6$) and vitiligo ($n = 9$) mice. Each column represents a biological replicate. (**B**) Krona [48] circle diagram illustrating the mean percent of taxa at the different levels of *Clostridiales* in non-induction ($n = 6$) and vitiligo ($n = 9$) mice. (**C**) Linear discriminant analysis effect size (LEfSe) [27] analysis showing significantly different bacterial taxa at various levels in control mice relative to vitiligo mice. (**D**) Relative abundance of differentially abundant taxa at the *phylum* level for control ($n = 6$) and vitiligo ($n = 9$) mice. Mean and SEM. (**E**) Relative abundance of differentially abundant taxa at the *genus* level for control ($n = 6$) and vitiligo ($n = 9$) mice. Mean and SEM. Statistical significance was determined using (E and F) Mann-Whitney *U* test. $*P < 0.05$, $**P < 0.01$, $***P < 0.001$.

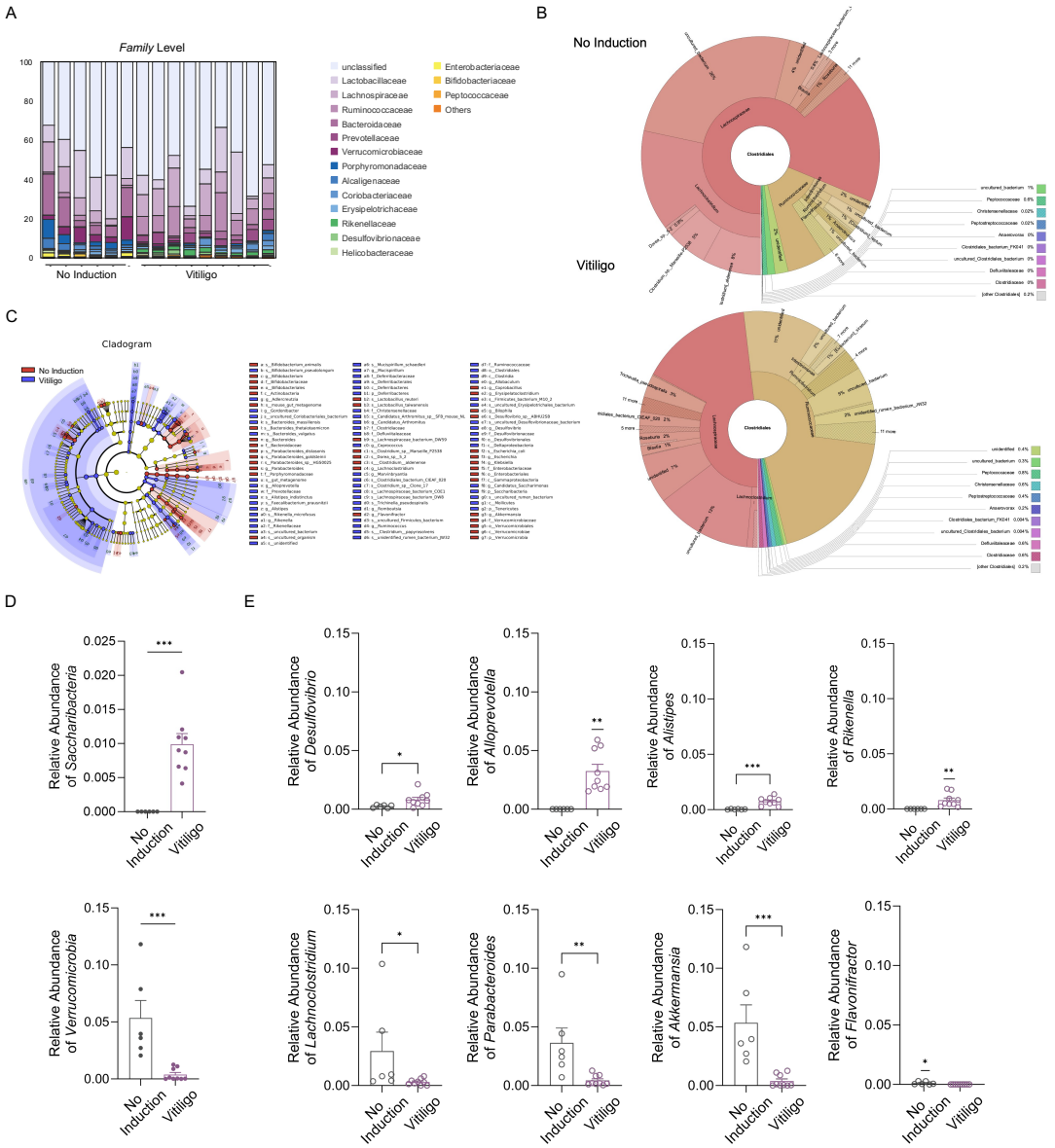

Fig. S5. Metabolomics signature of vitiligo mice in fecal, serum, and skin after melanoma-Treg-induced vitiligo model. (**A** and **B**) Multivariate control chart (MCC) and principal component analysis (PCA) of metabolites in fecal, serum, and skin tissues from non-induction and vitiligo mice treated with water and ABX. Batch correction with pooled quality controls (QCs) was performed to normalize batch-to-batch variability before further data analysis. Each dot in the MCC represents an individual sample. (**C**) Pathway enrichment analysis bar plot using pathway-associated metabolite sets (SMPDB): comparison of non-induction versus vitiligo mice in fecal, serum, and skin tissues. (**D** and **E**) Quantification of 2-phenylpropionate, hippuric acid, and indoleacetic acid in fecal and skin tissues of non-induction ($n = 6$) and vitiligo ($n = 6$) mice. Mean and SEM. Statistical significance was determined using (D and E) Mann-Whitney U test. $^{*}P < 0.05$, $^{**}P < 0.01$.

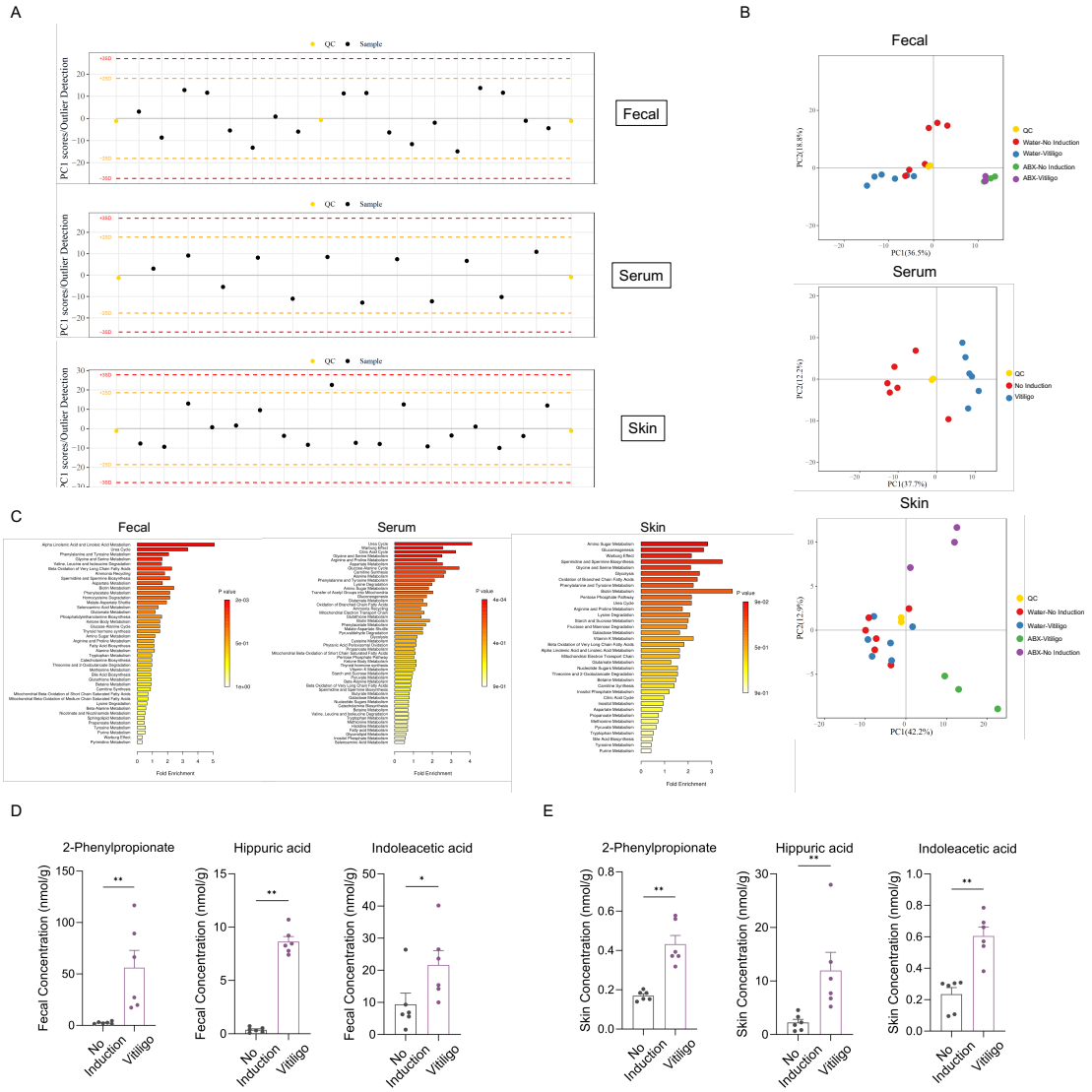

Fig. S6. Hippuric acid-related oxidative stress genes signature and gut-blood barrier signature in vitiligo mice. (**A**) Representative confocal images and quantification of mean dihydroethidium (DHE) fluorescence intensities showing reactive oxygen species (ROS) levels in tail skin sections from non-induction and vitiligo mice treated with 2-phenylpropionate (2-PP) or indoleacetic acid (IAA), $n = 4$ mice/group. Scale bars, 200 μm. (**B**) Combined data showing the quantification of mean DHE fluorescence intensities showing ROS levels in tail skin sections from non-induction and vitiligo mice treated with vehicle, 2-PP, HA, or IAA. Data were pooled from 3 independent experiments with $n = 4$ mice per group. (**C**) Representative wholemount immunofluorescent staining of tail epidermis images of vitiligo mice showing Melan-A^+ melanocytes and $CD8^+$ T cells treated intraperitoneally with the vehicle and HA daily from Day 12 to Day 35 during the vitiligo induction procedure. (**D**) Quantification of Melan-A^+ melanocytes and $CD8^+$ T cells in the epidermis of vitiligo mice treated intraperitoneally with vehicle ($n = 4$) and HA ($n = 4$). (**E**) Quantification of HA concentration in human serum samples from healthy volunteers ($n = 15$) and vitiligo patients ($n = 15$) using targeted metabolite analysis. (**F**) Heatmap of ROS-related genes in the tail skin of wild-type mice treated intraperitoneally with vehicle ($n = 3$) and HA ($n = 5$). Each column represents a biological replicate. (**G**) Representative histology of the large intestine using H&E and Alcian blue staining of non-induction and vitiligo mice. Scale bars, 50 μm. (**H** and **I**) Representative immunohistochemical staining images and quantification of mean H-score of Zonula Occludens-1 (ZO-1) and Occludin in the small intestine of non-induction ($n = 3$) and vitiligo mice ($n = 4$). Scale bars, 50 μm. (**J**) Relative abundance of gut mucin degradation-related taxa for non-induction ($n = 9$) and vitiligo ($n = 9$) mice. Mean and SEM. (**K**) Schematic diagram illustrating the translocation of hippuric acid into the circulation 4 hours post-oral gavage in non-induction and vitiligo mice treated with water and ABX. Statistical significance was determined using using (B) one-way ANOVA followed by Tukey's post-hoc test, using (C and D) unpaired Student's *t*-test, using (I) Mann-Whitney *U* test and. $*P < 0.05$, $**P < 0.01$, $***P < 0.001$.

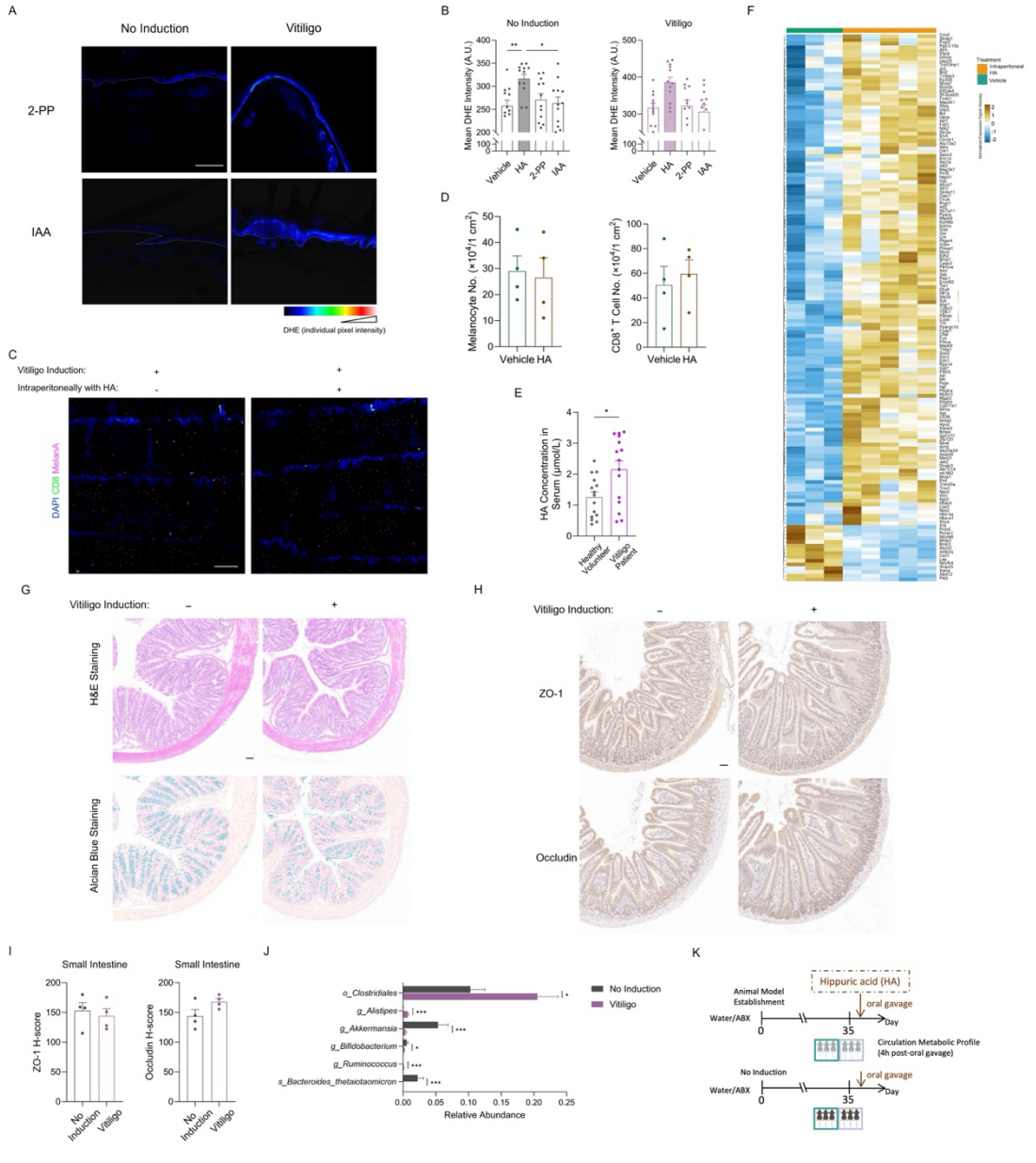
A
No Induction
Vitiligo
2-PP
IAA
DHE (individual pixel intensity)
B
No Induction
Vitiligo
Mean DHE Intensity (A.U.)
Vehicle
HA
2-PP
IAA
C
Vitiligo Induction:
Intraperitoneally with HA:
DAPI CD8 MelanA
D
Melanocyte No. (×10⁴/1 cm²)
CD8⁺ T Cell No. (×10⁴/1 cm²)
Vehicle HA
E
HA Concentration in Serum (μmol/L)
Healthy Volunteer
Vitiligo Patient
F
Treatment
Intraperitoneal
HA
Vehicle
G
Vitiligo Induction:
H&E Staining
Alcian Blue Staining
H
Vitiligo Induction:
ZO-1
Occludin
I
Small Intestine
ZO-1 H-score
Occludin H-score
No Induction
Vitiligo
J
o_Clostridiales
g_Alistipes
g_Akkermansia
g_Bifidobacterium
g_Ruminococcus
s_Bacteroides_thetaiotaomicron
No Induction
Vitiligo
Relative Abundance
K
Hippuric acid (HA)
Animal Model Establishment
oral gavage
Water/ABX
Day
Circulation Metabolic Profile (4h post-oral gavage)
No Induction

Fig. S7. Quality control results and steady-state analysis of proteins combined with hippuric acid for DSF and SPR. (**A**) Sodium dodecyl sulfate-polyacrylamide gel electrophoresis (SDS-PAGE) electrophoresis image showing myeloperoxidase (MPO), mitogen-activated protein kinase 14 (MAPK14), and nitric oxide synthase 2 (NOS2) protein quality. (**B**) The bicinchoninic acid (BCA) protein assay standard curve was used to determine protein concentrations. (**C**) Steady-state analysis based on response values detected at equilibrium. The fitted saturation curves demonstrate that as the concentration of the small molecule increases, the response values for MPO and NOS2 proteins also increase, indicating an increased amount of ligand captured by the proteins.